Petroleum Science 21 (2024) 2089–2101

Contents lists available at ScienceDirect

Petroleum Science

journal homepage: www.keaipublishing.com/en/journals/petroleum-science

Original Paper

Acid-rock reaction kinetics in a two-scale model based on reaction order correction

Xue-Song Li [a], Ning Qi [a, b, *], Ze-Hui Zhang [a], Lian Liu [c], Xia-Qing Li [d], Xu-Hang Su [a]

[a] School of Petroleum Engineering, China University of Petroleum (East China), Qingdao, 266580, Shandong, China
[b] Key Lab of Unconventional Oil & Gas Development, Ministry of Education, China University of Petroleum (East China), Qingdao, 266580, Shandong, China
[c] SINOPEC Northwest Oilfield Branch Company, Urumqi, 830011, Xinjiang, China
[d] Petroleum Engineering Technology Research Institute, SINOPEC Shengli Oilfield Company, Dongying, 257000, Shandong, China

ARTICLE INFO

Article history:
Received 16 March 2023
Received in revised form
18 July 2023
Accepted 21 November 2023
Available online 25 November 2023

Edited by Jia-Jia Fei and Min Li

Keywords:
Reaction order
Two-scale model
Wormhole propagation
Carbonate rocks
Numerical simulation

ABSTRACT

The reaction order plays a crucial role in evaluating the response rate of acid-rock. However, the conventional two-scale model typically assumes that the reaction order is constant as one, which can lead to significant deviations from reality. To address this issue, this study proposes a novel multi-order dynamic model for acid-rock reaction by combining rotating disk experimental data with theoretical derivation. Through numerical simulations, this model allows for the investigation of the impact of acidification conditions on different orders of reaction, thereby providing valuable insights for on-site construction. The analysis reveals that higher response orders require higher optimal acid liquid flow rates, and lower optimal H^+ diffusion coefficients, and demonstrate no significant correlation with acid concentration. Consequently, it is recommended to increase the displacement and use high-viscosity acid for reservoirs with high calcite content, while reducing the displacement and using low-viscosity acid for reservoirs with high dolomite content.

1. Introduction

Matrix acidizing is a common measure to increase production in carbonate reservoirs, and the rate of acid-rock reaction and rock dissolution pattern are important factors affecting the effect of reservoir acidizing. By studying the kinetics of acid-rock reaction, we can analyse the influencing factors of acid-rock reaction and the variation of rock pore-permeability during the process of acidizing, so as to develop a more efficient and low-cost acidizing plan.

Previous studies have investigated various factors affecting acid-rock reactions such as the optimal acid injection rate (Ma et al., 2022; Dong, 2018; Su et al., 2022), mineral composition (Martyushev et al., 2022), acid concentration (Chen et al., 2020), temperature (Zhou et al., 2022; Liu et al., 2019), acid viscosity (Mahmoodi et al., 2018), pH (Yoo et al., 2018) and type of acid system (Guo et al., 2020; Martyushev and Vinogradov, 2021; Yan et al., 2019). It is generally accepted that rock erosion morphology is controlled by two processes: acid transfer and acid-rock reaction (Wei et al., 2019; Dos Santos Lucas et al., 2022; Maheshwari et al., 2013). When the H^+ mass transfer rate and acid-rock reaction rate are relatively balanced, the rock dissolution morphology exhibits a wormhole type dissolution characteristic (Hoefner and Fogler, 1989; Qiu et al., 2018). Under the wormhole dissolution morphology, the pore acidification breakthrough volume ratio is the minimum (Papamichos et al., 2020; Qi et al., 2017), and the acid utilization efficiency is the highest. The injection rate corresponding to the smallest breakthrough volume ratio is also known as the optimal acid injection rate (Lohrasb et al., 2022; Qi et al., 2018; Dos Santos Lucas et al., 2022).

In order to describe more accurately and intuitively the changes in acid-rock reaction rates and rock porosity fields during acidification, researchers have proposed a variety of numerical models for acidification on an experimental basis. The early numerical models described the acid-rock reaction process by defining dimensionless numbers (e.g., Damköhler model (Fredd and Miller, 2000) and Peclet model (Al-Arji et al., 2021; Sahu et al., 2022)), while later capillary models assumed that wormhole was cylindrical capillaries that could grow radially and axially (Hung et al., 1989; Buijse, 2000). The network model uses pores as network nodes to

* Corresponding author. School of Petroleum Engineering, China University of Petroleum (East China), Qingdao, 266580, Shandong, China.
E-mail address: qining@upc.edu.cn (N. Qi).

https://doi.org/10.1016/j.petsci.2023.11.023

simulate rock dissolution by calculating the change in pore volume and throat radius at different times (Fatt, 1956; Tansey and Balhoff, 2016; Algive et al., 2010). However, it is difficult to apply to large-scale calculations at real mine sites due to the huge computational effort. The most widely used numerical model for acidification is the two-scale continuous medium model (Liu et al., 1997; Panga et al., 2005; Dong et al., 2021), which consists of two parts: a Darcy-scale model describing fluid flow and chemical reactions and a pore-scale model describing changes in reservoir properties. The two-scale model has good accuracy of results and stability of solutions at different time steps (Jia et al., 2021; Wang et al., 2020), but its computational complexity and the fact that all acid-rock reactions are by default primary reactions affect the accuracy of the results.

In the numerical model of the acid-rock reaction, the number of reaction order is related to the acid-rock reaction rate in power law, the higher the number of reaction order, the greater the influence of the change in acid concentration on the acid-rock reaction rate. When the number of reaction order is zero, changes in acid concentration will no longer affect the acid-rock reaction rate, and carbonate reservoirs are commonly acidified with a hydrochloric acid-based system, so the range of acid-rock reaction orders for carbonate rocks are often between zero and three (Ma et al., 2020; Abdelgawad et al., 2019; Tabasy and Rashidi, 2015). Although a number of previous numerical models of acid flow have approximated the acid concentration and reaction rate as linear (the number of reaction order is approximated as 1) (Bickle, 1992; Skelton et al., 1997; Skelton, 2011), subsequent research has shown that the chemical reaction rate between acid fluids and carbonate minerals is more often non-linear, the number of reaction order is often in the form of a fractional number (Lasaga, 1986; Baxter and DePaolo, 2002; Morse et al., 2007). Therefore, a multi-order acid-rock reaction model will provide a more accurate description of the non-linear relationship between concentration and acid-rock reaction rate in most practical situations, which will help to predict the rate variation of the carbonate rock dissolution process in a more refined way, and thus make a more rational planning of acidizing acid dosage and acid system preference.

The most common methods used to analyse experimental data on reaction orders are the integral and differential methods (Chen, 2000). The integral method was first proposed by Wilhelmy as an experimental extension of the law of action of acids on sucrose (Wilhelmy, 1850), where the acid concentration-reaction time data are brought into the kinetic equations of different orders to find the reaction order with the best fit, but the calculation is more complicated when the number of reaction order is not an integer. The differential method was first proposed by Hoff (1884), where the number of reaction order was obtained by logarithmically fitting the acid concentration-reaction time data to a regression. The differential method allows the reaction rate to be investigated as a function of time for a given initial reactant concentration and allows the law of variation of the number of reaction order to be deduced, which will be used as the method of analysis of the number of reaction order in this paper.

This paper focuses on the effect of variation in the number of reaction orders on the acidification reaction of carbonate rocks. Firstly, the acid concentration-reaction rate data of carbonate rocks with different mineral fractions reacting with hydrochloric acid were measured by rotating disk experiments, and the number of reaction orders and surface reaction rate constants of carbonate rocks with different mineral fractions were obtained by the differential method. Secondly, based on the experimental data and theoretical derivation of the rotating rock disk, a numerical model of acidification applicable to multi-order acid-rock reactions was established based on the traditional two-scale continuous medium model, which reduces the errors caused by the traditional model due to the approximation of the number of reaction orders. Finally, the influence of the number of reaction order on the acid-rock reaction under different acidification conditions (acid injection rate, H^+ diffusion coefficient, acid concentration) was investigated by numerical simulation, and the variation of the optimum injection rate and the optimum H^+ diffusion coefficient under different reaction orders were analysed. The study results suggest a strategy for acidizing the reservoirs with different dolomite and limestone contents in terms of discharge adjustment and acid system preference.

2. Experimental

In this paper, the reaction rates of carbonate rocks with different mineral fractions and different concentrations of hydrochloric acid were measured by rotating disc experiments, and the reaction orders and acid-rock reaction rate constants of carbonate rocks with different mineral fractions and hydrochloric acid were obtained to provide a parameter basis for subsequent numerical simulations.

2.1. Materials

Rock samples with 96% calcite content were used as pure limestone samples and rock samples with 96% dolomite content were used as pure dolomite samples. The experimental materials are shown in Table 1.

The experimental apparatus and equipment are shown in Table 2.

2.2. Experiment methods

The expression for the rate of acid-rock reaction in a rotating disk is

$$J = kC^m \tag{1}$$

where, J is the acid-rock reaction rate, $mol \cdot s^{-1} \cdot cm^{-2}$; k is the multi-order acid-rock reaction rate constant, $mol^{1-m} \cdot s^{-1} \cdot m^{3m-2}$; C is the acid concentration, $mol \cdot L^{-1}$; m is the number of reaction orders, no factor. Taking the logarithm of both sides of Eq. (1) gives.

$$\lg J = \lg k + m \lg C \tag{2}$$

The acid-rock reaction rate and concentration can be measured experimentally by plotting the curve with the logarithm of the concentration as the horizontal coordinate and the logarithm of the reaction rate as the vertical coordinate with a slope of m and an intercept of lg k.

The number of reaction orders and the reaction rate of the acid-rock reaction can be found in Eq. (2), which provides the parameters for the subsequent numerical simulation.

2.3. Results and discussion

Hydrochloric acid (5%, 10%, 15%, 20% mass fraction) was prepared with reference to the range of acid concentrations commonly used in mine acidizing construction, and the acid-rock reaction was carried out at a pressure of 7–8 MPa and a temperature of 90 °C. After experimental measurement of the critical disk rotation speed, the disk speed was set at 500 $r \cdot min^{-1}$, ensuring that the reaction process was surface reaction controlled. Based on the experimental data, the logarithmic relationship between the acid-rock reaction rate and acid concentration for carbonate rocks with different mineral fractions was plotted as shown in Fig. 1.

Table 1
Statistical table of experimental materials.

Experimental materials	Specification	Material sources
Hydrochloric acid	AR	Sinopharm Group Chemical Reagent Co.
Carbonate rocks	96% dolomite (pure dolomite)	Field coring of an oil field in Central Asia
	56% dolomite (grey dolomite)	
	96% Calcite (pure limestone)	Xinjiang outcrops
Deionized water	Electrical conductivity <0.5 us·cm^{-1}	Homemade

Table 2
Statistical table of experimental apparatus.

Instrument name	Manufacturers
Acid rock response rotating petrograph	Hai'an County Petroleum Research Instruments Co.
Automatic potentiometric titrator	Shanghai Yidian Scientific Instruments Co.
Electronic scales	Sartorius Research Instruments Co.

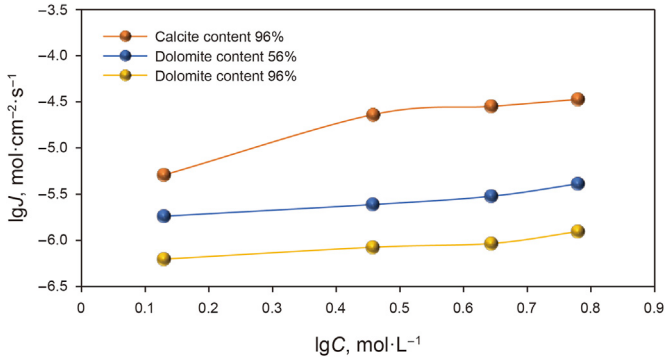

Fig. 1. Logarithmic plot of acid-rock reaction rate versus acid concentration for carbonate rocks (90 °C, 500 r·min^{-1}).

Fig. 1 shows that the reaction rates of carbonate rocks of different mineral fractions with hydrochloric acid all show the same trend as the acid concentration changes. That is, in the range of 5%–25% mass fraction of hydrochloric acid, the acid concentration increases and the reaction rate of acid-rock increases. This is due to the fact that during the acid-rock reaction, the mineral surface H^+ is continuously consumed and the concentration gradient of H^+ within the acid phase of the more concentrated hydrochloric acid solution to the rock surface is higher, hence the faster H^+ transfer rate.

The data in Fig. 1 and Eq. (2) show that the number of reaction order for 96% calcite, 56% dolomite, and 96% dolomite is 1.27, 0.92, and 0.42 respectively. The sensitivity of the acid-rock reaction to changes in acid concentration varies for different reaction order. The reason for this is that the higher the number of acid-rock reaction orders, the more calcite is present in the rock mineral fraction and the more H^+ is consumed to dissolve the same volume of rock under the same conditions. For the same incremental acid concentration, the greater the increase in acid-rock reaction rate and the more pronounced the deepening of non-uniform etching in carbonate rocks containing more calcite.

According to the conclusion of the experimental data, the experimentally measured reaction rate J of hydrochloric acid and acid-rock reaction rate of carbonate rocks with different mineral fractions and the acid concentration C were plotted in the same coordinate system, and the curve was fitted to the formula to obtain the number of acid-rock reaction orders and acid-rock reaction rate data, and the data were collated as shown in Table 3.

The difference in reaction order observed can be attributed to the difference in chemical composition between calcite and dolomite. Calcite is mainly composed of $CaCO_3$ while dolomite is composed of $CaMg(CO_3)_2$. The chemical reaction equations between these two minerals and hydrochloric acid are shown below.

$$CaCO_3 + 2HCl = CaCl_2 + CO_2\uparrow + H_2O \quad (3)$$

$$CaMg(CO_3)_2 + 4HCl = CaCl_2 + MgCl_2 + 2CO_2\uparrow + 2H_2O \quad (4)$$

Equations (3) and (4) demonstrate that the amount of hydrochloric acid required for calcite to react is half of that required for dolomite to react under the same concentration of hydrochloric acid. As a result, carbonate rocks with higher dolomite content exhibit lower reaction rates under the same reaction conditions. To illustrate this phenomenon, rock cores containing 4%, 56%, 75% dolomite, and 96% calcite were selected to perform acid-rock reaction experiments with hydrochloric acid of 20% mass fraction under conditions of a reaction temperature of 90 °C and a rotating speed of 500 r·min^{-1} of the rotating rock disk. The experimental results are presented in Fig. 2.

As shown in the experimental data, while other acidification conditions remain unchanged, the acid-rock reaction rate gradually decreases with the increase of dolomite content. According to Eqs. (3) and (4), under the same acidification conditions, reacting dolomite with the same volume consumes more acid than calcite, because the different chemical molecular formulas of the two lead to different reaction activity. The more active the reaction, the higher the sensitivity of minerals to changes in acid concentration. This is reflected in Eq. (1), which indicates that the higher the power of the acid concentration C, the higher the reaction order. Therefore, as the content of dolomite increases, the rate of acid-rock reaction gradually decreases, the activity of rock acidification reaction decreases, and the reaction order decreases accordingly.

3. Mathematical models

In this paper, acid erosion was investigated for acid flowing from the left inlet at a constant rate into a two-dimensional rectangular domain, which simulates a continuous rock matrix with no flow at

Table 3
Data on the number of acid-rock reaction orders and acid-rock reaction rates for different mineral fractions.

Mineral fraction	Acid-rock reaction order m	Acid-rock reaction rate k_s, × 10^{-6} m·s^{-1}
96% dolomitic carbonate rock	0.42	6.02
56% dolomitic carbonate rock	0.92	14.42
Carbonate rock with 96% calcite	1.27	41.95

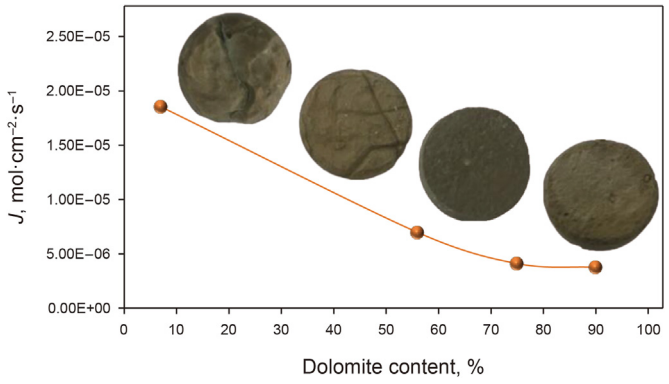

Fig. 2. Relationship between acid-rock reaction rate and logarithm of acid concentration in carbonate rocks (acid concentration 20%, 90 °C, 500 r·min^{-1}).

the upper and lower boundaries. The mathematical model was developed with reference to the improved two-scale continuous medium model by Panga et al. (2005), on which a multi-order acid-rock reaction model was constructed by considering the effect of reaction order variation on the reaction rate calculation results.

The multi-order acid-rock reaction model assumes that: (i) the dissolution process of the acid-rock reaction does not affect the liquid phase density and acid concentration, and that the formation fluid is saturated and incompressible; (ii) the effect of the heat given off by the acid-rock reaction on the ambient temperature is ignored; and (iii) the pore fluid viscosity is assumed to be approximately equal to the acid fluid viscosity, and the effects of gravity and capillary forces are ignored.

3.1. Mathematical model

3.1.1. Darcy scale model

The Darcy-scale model characterises the flow of acid in the formation and includes equations controlling the direction of acid flow (5); the effect of acid flow on rock porosity (6); the effect of acid-rock chemistry on rock porosity (7) and (9) and a defining equation for the source term of the acid-rock reaction kinetics (8).

$$\mathbf{U} = -\frac{1}{\mu}\mathbf{K}\cdot\nabla P \tag{5}$$

$$\frac{\partial \varepsilon}{\partial t'} + \nabla\cdot\mathbf{U} = 0 \tag{6}$$

$$\frac{\partial(\varepsilon C_s)}{\partial t'} + \nabla\cdot\left(\mathbf{U}C_f\right) = \nabla\cdot\left(\varepsilon\mathbf{D}_e\cdot\nabla C_f\right) - k_c a_v\left(C_f - C_s\right) \tag{7}$$

$$k_c\left(C_f - C_s\right) = R(C_s) \tag{8}$$

$$\frac{\partial \varepsilon}{\partial t'} = \frac{R(C_s)a_v\alpha}{\rho_s} \tag{9}$$

where $\mathbf{U}$ is the Darcy velocity vector; $\mathbf{K}$ is the permeability tensor; P is the pressure, Pa; ε is the porosity; C_f is the concentration of acid in the liquid phase, mol·L^{-1}; C_s is the concentration of acid at the liquid-solid interface, mol·L^{-1}; $\mathbf{D}_e$ is the effective diffusion tensor; k_c is the local mass transfer coefficient, m·s^{-1}; a_v is the interfacial area per unit volume of medium that can participate in the reaction m^2·m^{-3}; ρ_s is the density of the solid phase, kg·m^{-3}; α is the acid solubility, defined as the number of grams of solid dissolved per mole of reacting acid, g·mol^{-1}. The reaction kinetic function is expressed as $R(C_s)$. For primary reactions, the value of $R(C_s)$ depends on k_sC_s, where k_s is the surface reaction rate constant, m·s^{-1}.

3.1.2. Pore scale model

A complete kinetic model for acid-rock reactions needs to take into account parameters reflecting the porous media of carbonate rocks such as the permeability tensor $\mathbf{K}$, the effective diffusion tensor $\mathbf{D}_e$, the mass transfer coefficient k_c, and the specific surface area a_v as characteristic parameters. Therefore, as a characterisation of the reservoir pore properties, pore-scale models also need to be introduced into the model.

The pore-scale model uses semi-empirical relationships related to local porosity to characterise the intrinsic link between permeability, porosity, and interfacial reaction area and their initial values, as shown in Eqs. (10)–(12).

$$\frac{K}{K_0} = \frac{\varepsilon}{\varepsilon_0}\left(\frac{\varepsilon(1-\varepsilon_0)}{\varepsilon_0(1-\varepsilon)}\right)^{2\beta} \tag{10}$$

$$\frac{r_p}{r_0} = \sqrt{\frac{K\varepsilon_0}{K_0\varepsilon}} \tag{11}$$

$$\frac{a_v}{a_0} = \frac{\varepsilon r_0}{\varepsilon_0 r_p} \tag{12}$$

where ε is the porosity; ε_0 is the initial porosity; K is the local permeability, D; K_0 is the initial permeability, D; r_p is the average pore radius, m; r_0 is the initial average pore radius, m; a_0 is the initial specific surface area, m^2; a_v is the specific surface area, m^2; β is the pore structure-related constant.

3.2. Model modification

The multi-order acid-rock reaction model is corrected for the error between the theoretical $R(C_s)$ value calculated from the kinetic term of the acid-rock reaction of the traditional two-scale model $R(C_s) = k_sC_s^m$ (default $m = 1$) and the actual $R(C_s)$ value for a number of reaction order $m \neq 1$.

In this paper, this error will be reduced by discretizing the curve and fitting the function in segments. For acid-rock reactions in the range $0 < C_s \leq C_{seg}$ mol·L^{-1}, the standard 1-order reaction model will still be used; for acid-rock reactions in the range $C_s > C_{seg}$ mol·L^{-1}, the regression fitting method is chosen to obtain the modified function expressions. Since the acid-rock reaction function curve in this range is approximately linear, the expression for the reaction in the range $C_s > C_{seg}$ mol·L^{-1} is assumed to be as shown in Eq. (13) (for the number of reaction order $m = n$)

$$R_n'(C_s) = k_{sn}'C_s + R_n \tag{13}$$

where $R_n'(C_s)$ is the modified reaction kinetic function for a reaction order of n; k_{sn}' is the modified acid-rock reaction rate constant for a reaction order of n, m·s^{-1}; R_n is the modified reaction rate error constant, mol·m^{-2}·s^{-1}.

According to the method of least squares, it is known that the expression k_{sn}' in Eq. (14) is

$$k_{sn}' = \frac{\sum_{i=1}^{n} C_s R_{ni}'(C_s) - n\overline{C}_s\cdot\overline{R'}_n(C_s)}{\sum_{i=1}^{n} {C_s}^2 - n\overline{C}_s{}^2} \tag{14}$$

where $R_{ni}'(C_s)$ is the i-th data point of the modified reaction kinetic

function for a reaction order of n, $i = 1, 2, 3, \ldots$; $\overline{C}_s$ is the overall average of the acid concentrations within the data point phase, $mol \cdot m^{-3}$; $\overline{R}_n(C_s)$ is the overall average of the modified reaction kinetic function data points for a reaction order of n.

After determining k'_{sn}, according to the method of coefficients to be determined, since

$$\overline{R}'_n(C_s) = k'_{sn}\overline{C}_s + R_n \tag{15}$$

The R_n value was obtained. Next, determining the segmentation point C_{seg} for the piecewise function is crucial. To ensure continuity of the function, the intersection point between two curves is chosen as the segmentation point for the piecewise function.

This gives the corrected kinetic expression for the acid-rock reaction

$$R_n(C_s) = \begin{cases} k_{sn}C_s, 0 < C_s \le C_{seg} \\ k'_{sn}C_s + R_n, C_{seg} < C_s < C_{max} \end{cases} \tag{16}$$

The equation $R(C_s) = k_c(C_f - C_s)$ is then used to make an equivalence to obtain the modified multi-order reaction $C_f - C_s$. The relationship is

$$C_s = \begin{cases} \dfrac{C_f}{1 + \dfrac{k_{sn}}{k_c}}, 0 < C_s \le C_{seg} \\ \dfrac{C_f - R_n}{\dfrac{k'_{sn}}{k_c} + 1}, C_{seg} < C_s < C_{max} \end{cases} \tag{17}$$

The resulting modified two-scale continuous medium model expression for the multi-order acid-rock reaction is

$$\frac{\partial\left(\varepsilon C_f\right)}{\partial t'} + \nabla \cdot \left(\mathbf{U}C_f\right) = \nabla \cdot \left(\varepsilon \mathbf{D}_e \cdot \nabla C_f\right) + \text{source} \tag{18}$$

where the source term expression is

$$\text{source} = \begin{cases} -k_c a_v \dfrac{C_f}{1 + \dfrac{k_c}{k_{sn}}}, 0 < C_s \le C_{seg} \\ -k_c a_v \left(C_f - \dfrac{C_f - R_n}{\dfrac{k'_{sn}}{k_c} + 1} \right), C_{seg} < C_s < C_{max} \end{cases} \tag{19}$$

This results in a modified acid-rock reaction kinetic model for an arbitrary number of reaction order ($m = n$, $n \ge 0$) requiring only the number of acid-rock reaction order and the reaction rate.

3.3. Model validation

For the sake of validation, in this paper, order of reaction is considered in the classic 1-order model data of carbonate rock acidification numerical simulation (Panga et al., 2005) and the experiment part, but in the numerical simulation part, order of reaction is approximated to 1-order model data (Xue, 2017) for model validation. The validation model experimental parameters are shown in Table 4.

Pore breakthrough volume (PVBT) curve as shown in Fig. 3.

For the simulation of Fig. 3(a), it is only necessary to make the number of reaction orders $m = 1$ in this multi-order model, the surface reaction rate parameters k_s the same, for different intervals, make the reaction rate intercept $R_0 = 0$, and substitute the other parameters into the model to simulate the reaction of the classical 1-order model.

The curve data shows that when the default model parameters are first-order reaction parameters, the classic first-order model is highly similar to the multi-order model. The penetration volume ratio between the wormhole dissolution rate range and the uniform dissolution rate range of the two models is relatively close, and the minimum penetration volume ratio is reached at the same Da value, further proving the accuracy of the multi-order model. However, it is worth noting that in the range of surface dissolution rate, the control mode of acid rock reaction under low-speed flow is mainly mass transfer control mode. The presence of natural heterogeneity in the medium leads to an uneven increase in permeability along the leading edge. The difference in penetration volume ratio under low flow rates may be due to different random number settings of natural porosity in rock samples. Another possible reason for the difference is that Panga's paper uses the partial differential equation method after dimensionless processing of variables to solve the problem, while this paper uses the finite difference method to directly solve the parameters. The differences in this processing process may lead to subtle differences, but do not affect the final model solving conclusion.

The overall trend and range of values of the core breakthrough volume ratio curve in Xue's paper and the breakthrough volume ratio curve in this paper are similar, but because the experimentally obtained reaction order parameter is approximated to 1 in Xue's paper, the reaction rate obtained from the model calculation is slightly lower than the actual reaction rate (in 4.4 Correction analysis in the main text for details). The multi-order reaction model corrected for the number of reaction orders in this paper more accurately reflects the actual reaction rate at the acid rock surface, and the resulting breakthrough volume ratio minimum corresponds to a slightly higher injection rate than the value in Xue's paper. This conclusion is also consistent with the numerical modeling section of this thesis, for acid rock reactions with less than one order, using the classical one-order model will result in a higher optimum injection rate calculation; for acid rock reactions with more than one order, using the classical one-order model will result in a lower optimum injection rate calculation. The reason for this is the difference in accuracy between the classical model and the multi-order model in this paper in describing the rate of acid rock reactions.

3.4. Boundary and initial conditions

3.4.1. Boundary conditions

Acid is injected from the left-hand boundary perpendicular to the y-axis at a constant rate of acid flow.

$$U = U_0,\ x = 0 \tag{20}$$

$$C_f = C_0,\ x = 0 \tag{21}$$

where U_0 is the acid injection rate at the inlet, $m \cdot s^{-1}$; x is the x-axis coordinate of a point in the calculation domain, m; C_f and C_0 are the in-phase and inlet concentrations of the acid, $mol \cdot L^{-1}$, respectively.

The right-hand boundary pressure and the acid concentration gradient are constant at zero during the calculation and the equilibrium is broken when the acid breakthrough is completed.

$$P = P_e,\ x = L \tag{22}$$

Table 4
Multi-order model validation parameter settings.

Parameter	Value	Unit	Practical significance
λ_X	0.5	1	Longitudinal pore structure coefficient
λ_T	0.1	1	Transverse pore structure coefficient
Sh_∞	3.36	1	Asymptotic Sherwood number
K_0	10	mD	Initial permeability
A	0.5	1	Aspect ratio
φ_0	0.2	1	Average porosity
$\Delta\varphi$	0.15	1	Porosity variation
a_0	50	cm^{-1}	Interfacial area
r_0	1×10^{-6}	m	Initial pore radius
α_{os}	0.5		Pore-structure constant
ρ_{L_Panga}	1.2	$g \cdot cm^{-3}$	Acid density (Data via Panga et al. (2005))
ρ_{L_Xue}	1.08	$g \cdot cm^{-3}$	Acid density (Data via Xue (2017))
ρ_{s_Panga}	2.7	$g \cdot cm^{-3}$	Rock density (Data via Panga et al. (2005))
ρ_{s_Xue}	2.8	$g \cdot cm^{-3}$	Rock density (Data via Xue (2017))
μ_{Panga}	1	$MPa \cdot s^{-1}$	Kinematic viscosity (Data via Panga et al. (2005))
μ_{Xue}	3.6	$MPa \cdot s^{-1}$	Kinematic viscosity (Data via Xue (2017))
D_{m_Panga}	4×10^{-10}	$m^2 \cdot s^{-1}$	Molecular diffusion coefficient (Data via Panga et al. (2005))
D_{m_Xue}	3×10^{-9}	$m^2 \cdot s^{-1}$	Molecular diffusion coefficient (Data via Xue (2017))
k_{s_Panga}	1.4×10^{-5}	$m \cdot s^{-1}$	Surface reaction rate constant (Data via Panga et al. (2005))
k_{s_Xue}	5.07×10^{-5}	$m \cdot s^{-1}$	Surface reaction rate constant (Data via Xue (2017))
L_{Panga}	3.5	cm	Length of the core (Data via Panga et al. (2005))
L_{Xue}	5	cm	Length of the core (Data via Xue (2017))
M	1.202		Reaction order
k_s'	7.78×10^{-5}	$m \cdot s^{-1}$	Segmented acid rock reaction rate
R_0	-3.87×10^{-5}	$mol \cdot m^{-2} \cdot s^{-1}$	Multistage reaction intercept parameter

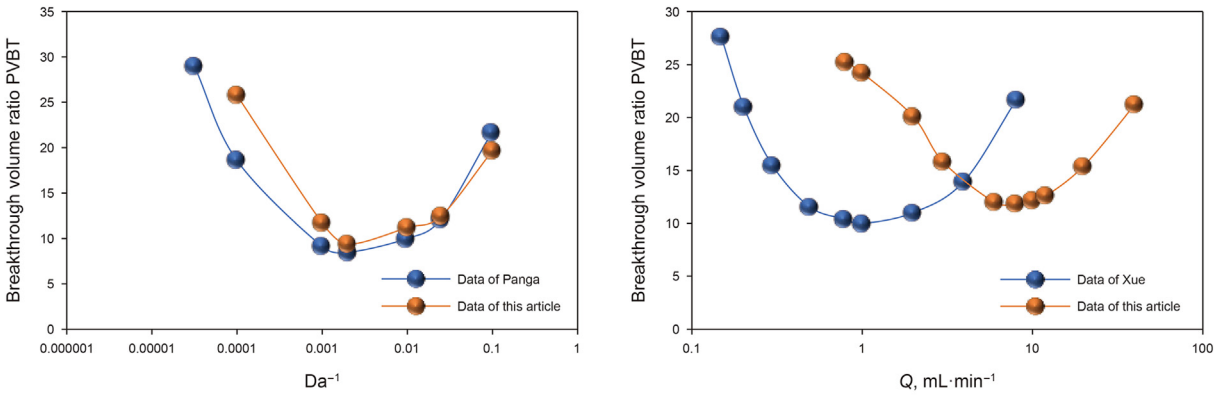

(a) Verification of Classic 1-order Model **(b)** Verification of Multi-order Model

Fig. 3. Model validation breakthrough volume ratio curve (**(a)** data derive from Panga et al. (2005); **(b)** data derive from Xue (2017)).

$$\frac{\partial C_f}{\partial x} = 0,\ x = L \tag{23}$$

where P is the pressure value at a point in the calculation domain, Pa; P_e is the boundary pressure value, Pa; L is the length scalar of the fluid flowing along the x-axis, m.

The upper and lower boundaries of the calculation domain are closed boundaries with no acid entry or exit.

$$-K\frac{\partial P}{\partial y} = 0,\ y = 0,\ y = H \tag{24}$$

$$\frac{\partial C_f}{\partial y} = 0,\ y = 0,\ y = H \tag{25}$$

where, K is the permeability at a point in the calculation domain, m^2; H is the y-axis coordinate of the upper boundary, m.

3.4.2. Initial conditions

Assuming that no acid exists in this computational domain at time $t = 0$.

$$C_f = 0,\ t = 0 \tag{26}$$

Assuming that the static pressure in this calculation domain is zero at time $t = 0$.

$$P = P_0,\ t = 0 \tag{27}$$

3.5. Geometric models

A rectangular geometry model of 10 cm in length and 5 cm in width was chosen for the numerical simulation part of this paper to carry out subsequent simulations. The Delaunay triangular mesh was used to delineate the grid, with cell sizes ranging from 1×10^{-1} to 2×10^{-3} cm. The random seeding method was used to simulate the inhomogeneous properties of the carbonate reservoir. The

specific geometric model and grid division figures are shown in Figs. 4 and 5.

3.6. Model parameters

The values of the numerical model parameters are shown in Table 5.

4. Numerical simulation

The parameters obtained from the rotating disk experiment were used to obtain k'_{sn}, the R_n in Eq. (11) using the number of reaction orders, and then the reaction rate constants were substituted into Eq. (17) to construct a multi-order numerical model of the acid-rock reaction at different orders. By varying the acid injection rate, H^+ diffusion coefficient, and acid concentration, the porosity field and pore breakthrough volume (PVBT) ratio curves of the multi-order acid-rock reaction under different acidification conditions were obtained, and the effect of the number of reaction order on the acid-rock reaction under different reaction conditions was investigated accordingly to advise on the field construction.

4.1. Injection speed

The distribution pattern of dissolution porosity for the multi-order acid-rock response model at different injection rates is shown in Figs. 6–9.

Based on the numerical simulation results, it can be seen that for any number of acid-rock reaction orders, the dissolution pattern changes from surface dissolution to wormholing dissolution to uniform dissolution as the injection rate increases. However, at lower injection rates (e.g., Figs. 6 and 7), the higher the number of reaction order, the coarser the wormholes and the poorer the development of branching wormholes, the closer to conical dissolution; at higher injection rates (e.g., Figs. 8 and 9), the lower the number of reaction order, the finer the wormholes and the more blurred the boundary between the wormholes and the undissolved matrix, the closer to uniform dissolution.

A plot of the acid injection rate vs. breakthrough volume ratio for the different orders of the acid-rock reaction is shown in Fig. 10.

In Fig. 10, the 1.27, 0.92, and 0.42 reaction curves are based on the multi-order acid-rock reaction model of this paper, while the 1-order reaction curve is based on the 0.92 acid-rock reaction rate constant, which is simulated by the traditional 1-order model. The optimum injection rate of the traditional 1-order acid-rock reaction kinetic model in Fig. 10 is significantly higher, partly because the parameters used in the 1-order acid-rock reaction model are the

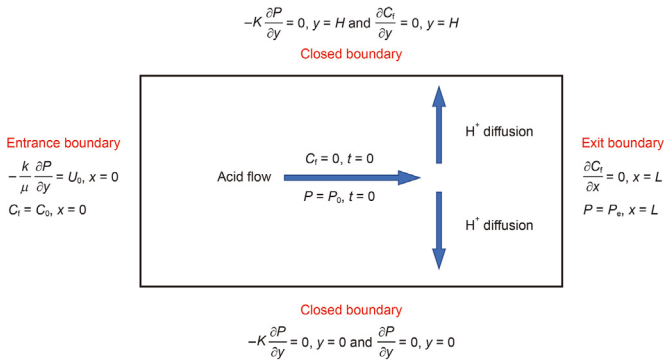

Fig. 4. Geometric diagram of the multi-order acid-rock reaction model.

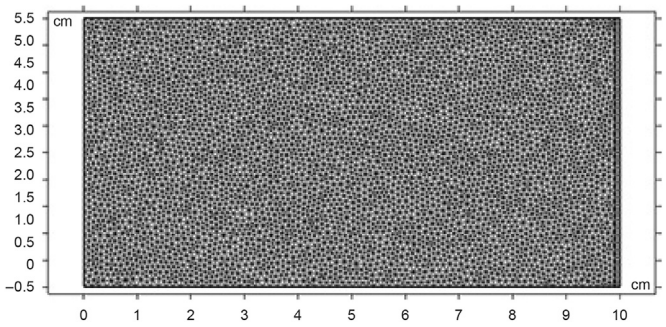

Fig. 5. Multi-order acid-rock reaction model meshing.

Table 5
Table of values for numerical simulation model parameters.

Parameters	Numerical values
Reservoir initial porosity K_0, mD	10
Initial concentration of acid C_0, mol·L^{-1}	4.4
Calculation of the domain length L, m	10
Calculation domain width H, m	5
Initial porosity ε_0	0.1
Initial pressure P_0, Pa	1×10^5
Pore structure parameter β	1
Acid solubility α, g·mol^{-1}	50
Transverse pore structure factor λ_x	0.5
Longitudinal pore structure factor λ_T	0.1
Initial pore radius r_0, m	4×10^{-6}
Initial specific surface area a_0, m^2·m^{-3}	5000
Density of the acid ρ_L, kg·m^{-3}	1200
Rock matrix density ρ_S, kg·m^{-3}	2700
Progressive Sherwood Number Sh_∞	3.66
Pore structure constant α_{os}	0.5

experimental parameters of the 0.92 acid-rock reaction, and partly because the 1-order acid-rock reaction model ignores the variation of the number of reaction orders, resulting in high surface reaction rate results. Further error analysis will be presented in Section 4.4.

When the breakthrough volume ratio is minimal, the axial advance velocity dominated by acid convection is relatively balanced with the radial expansion velocity dominated by acid-rock reaction, at which point the corresponding dissolution pattern is wormholing dissolution (Qi et al., 2018). As can be seen from the data in Fig. 10, the optimum acid injection rate increases with the number of acid-rock reaction orders. This is due to the fact that the higher the number of acid-rock reaction orders, the higher the calcite content of the rock, the higher the acid-rock surface reaction rate, and the higher the injection rate required to form wormholing dissolution (as shown in Fig. 11).

Based on the above conclusions, the higher the calcite content of the target reservoir, the higher the acid injection rate should be; the higher the dolomite content of the target reservoir, the lower the acid injection rate should be.

4.2. H^+ diffusion coefficient

The distribution pattern of dissolution porosity for the multi-order acid-rock reaction model with different H^+ diffusion coefficients is shown in Figs. 12–15.

Based on the numerical simulation results, it can be seen that for any number of acid-rock reaction orders, the rock dissolution pattern changes from uniform dissolution to wormholing dissolution to face dissolution as the diffusion coefficient of H^+ increases. The difference is that when the diffusion coefficient of H^+ is low (Figs. 12 and 13), the lower the number of reaction orders, the finer

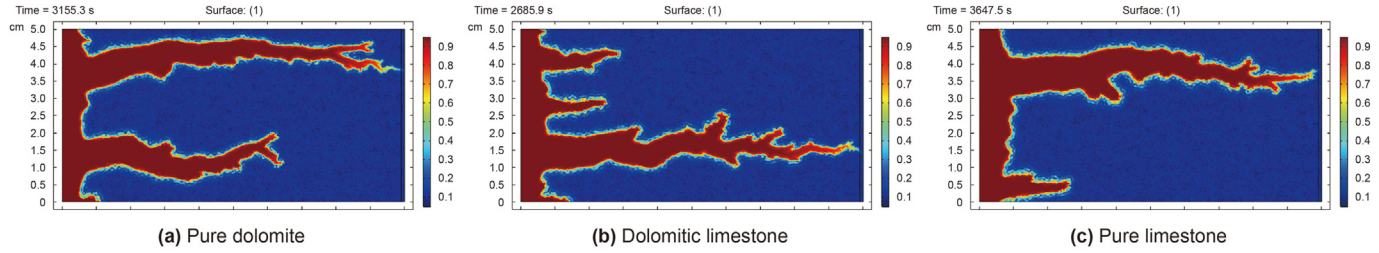

Fig. 6. Acid erosion porosity field for different orders of acid-rock reaction ($U_0 = 7.5 \times 10^{-5}$ m·s^{-1}).

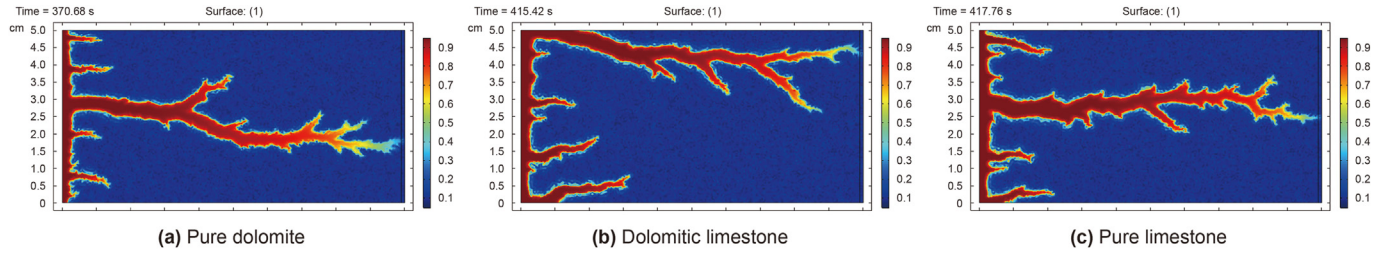

Fig. 7. Acid erosion porosity field for different orders of acid-rock reaction ($U_0 = 3 \times 10^{-4}$ m·s^{-1}).

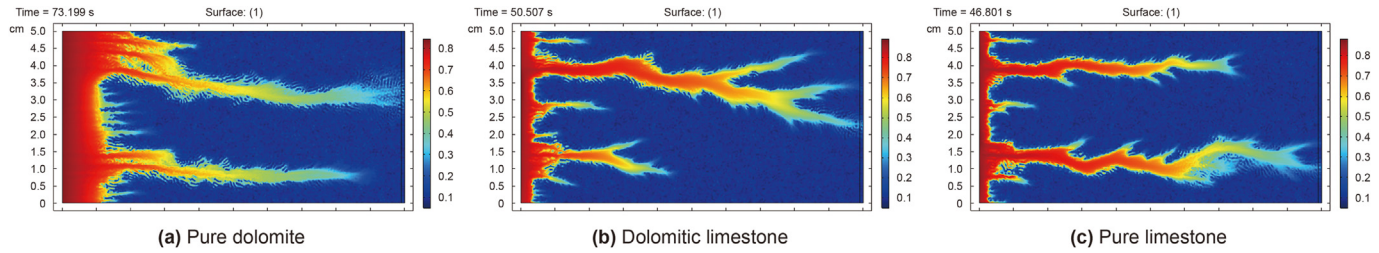

Fig. 8. Acid erosion porosity field for different orders of acid-rock reaction ($U_0 = 3 \times 10^{-3}$ m·s^{-1}).

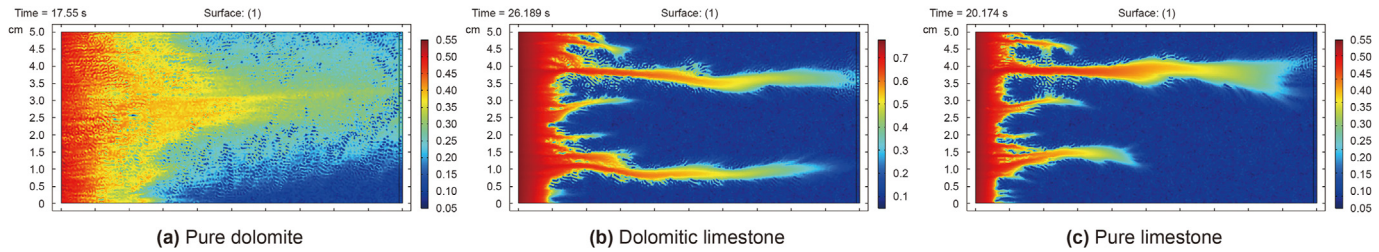

Fig. 9. Acid erosion porosity field for different orders of acid-rock reaction ($U_0 = 7.5 \times 10^{-3}$ m·s^{-1}).

the wormhole, the more blurred the boundary between the wormholes and the undissolved matrix, and the closer to uniform dissolution; when the diffusion coefficient of H^+ is high (Figs. 14 and 15), the higher the number of reaction orders, the coarser the wormhole, the less developed the wormhole branching, and the closer to conical dissolution.

The relative relationship between the diffusion coefficient and the breakthrough volume ratio for different orders of acid-rock reactions H^+ is shown in Fig. 16.

Fig. 16 shows that the optimum H^+ diffusion coefficient decreases as the number of acid-rock reaction orders increases. The reason for this is that the higher the number of reaction orders, the higher the calcite content of the rock and the faster the acid-rock surface reaction rate. In order to balance the acid convection rate with the acid-rock reaction rate, a smaller H^+ mass transfer rate is required to limit the acid-rock reaction rate, as shown in Fig. 17.

Therefore, the H^+ diffusion coefficient can be limited by increasing the acid viscosity, and using a slow acid system (e.g., thickening acid, emulsifying acid, etc.) when acidizing high calcite content reservoirs, while the H^+ diffusion coefficient can be increased by decreasing the acid viscosity when acidizing high dolomite content reservoirs.

4.3. Acid concentration

The distribution pattern of dissolution porosity for the multi-order acid-rock reaction model at different acid concentrations is shown in Figs. 18–21.

Based on the numerical simulation results, it can be seen that for any number of orders of acid-rock reaction, the variation in acid

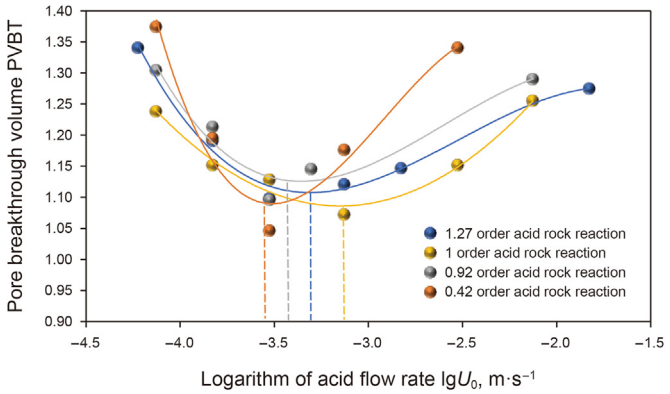

Fig. 10. Multi-order acid-rock reaction injection rate vs. breakthrough volume ratio curve.

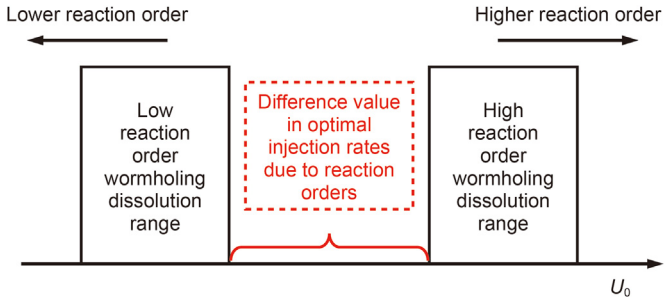

Fig. 11. Diagram showing the relationship between the dissolution pattern of the multi-order acid-rock reaction and the range of injection rates.

concentration does not have a significant effect on the dissolution pattern within the range of acid concentrations commonly used in acidizing construction (5%–25% mass fraction). The acid concentration to breakthrough volume ratio curve was plotted for analysis, as shown in Fig. 22.

As can be seen from Fig. 22, at lower acid concentrations (less than 5 mol·L^{-1}), the breakthrough volume ratio of different orders of acid-rock reaction decreases with increasing acid concentration; when the acid concentration is higher (greater than 5 mol·L^{-1}), the acid breakthrough volume ratio gradually tends to a stable value, at which time further increasing the acid concentration will have no significant effect on improving the acidification efficiency. The reason for this phenomenon is that the increase in acid concentration improves the mass transfer efficiency of H^+ and increases the acid-rock reaction rate. However, the main factor determining the mass transfer capacity of H^+ is the acid convection intensity, so as the acid concentration increases, the increase in acid-rock reaction rate decreases and the breakthrough volume ratio plateaus.

For the use of hydrochloric acid for the modification of carbonate reservoirs, if the acid concentration is below 5 mol·L^{-1}, the acid concentration can be increased to obtain a higher acidification efficiency. For concentrated acid acidification systems, changing the acid concentration has little effect on the dissolution pattern and acidification efficiency.

4.4. Correction analysis

The comparison diagram of the reaction rate curve of 0.42, 0.92, and 1.27 order acid-rock reaction before and after modification is shown in Figs. 23–25, with the aim of illustrating the quantitative analysis of the correction effect of the multi-order acid-rock reaction model.

The present study utilizes the R^2 score to quantitatively evaluate the efficacy of the modified multi-order acid-rock reaction model. The R^2 score, which ranges from negative infinity to 1, is a measure of the degree of conformity between the fitted data and the actual data (Waldmann, 2019; Chang et al., 2022; Kamble et al., 2021). A value between 0 and 1 indicates a high level of concurrence, while a negative R^2 score suggests a significant deviation in the fitted results and calls for a change in the fitting methodology. The calculation formula for the R^2 score is provided below.

$$R^2 = 1 - \frac{\sum_{i=1}^{n} (y_i - \hat{y}_i)^2}{\sum_{i=1}^{n} (y_i - y^2)^2} \tag{28}$$

where y_i is the actual acidification rate value, mol·cm^{-2}·s^{-1}; y^2 is

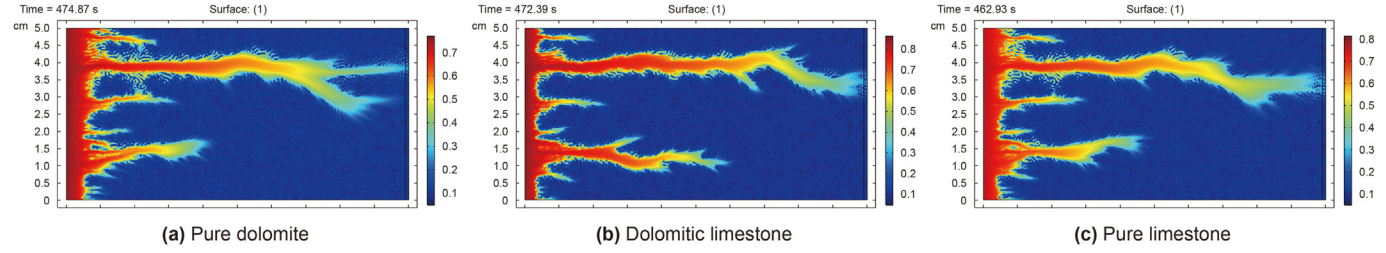

Fig. 12. Acid erosion porosity field for different orders of acid-rock reaction ($D_m = 1.5 \times 10^{-10}$ m^2·s^{-1}).

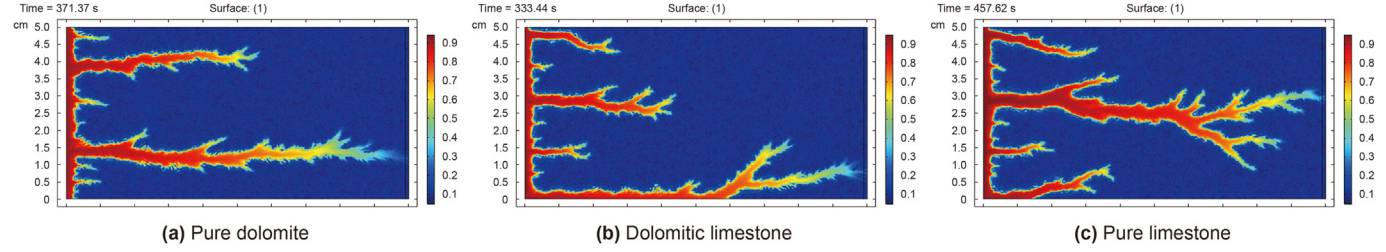

Fig. 13. Acid erosion porosity field for different orders of acid-rock reaction ($D_m = 9 \times 10^{-10}$ m^2·s^{-1}).

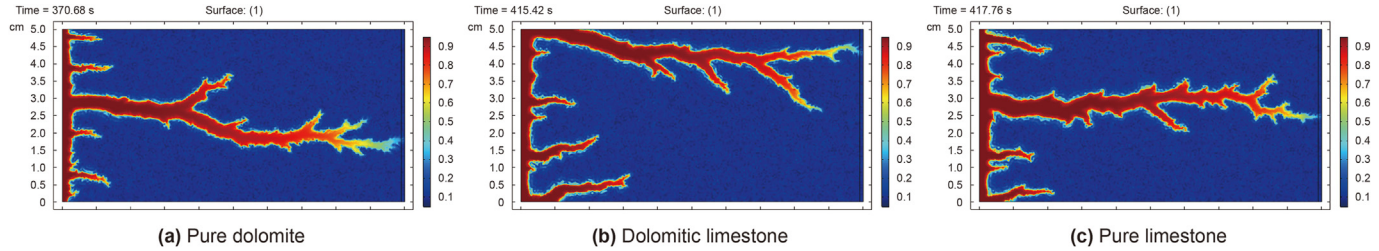

Fig. 14. Acid erosion porosity field for different orders of acid-rock reaction ($D_m = 3 \times 10^{-9}$ m^2·s^{-1}).

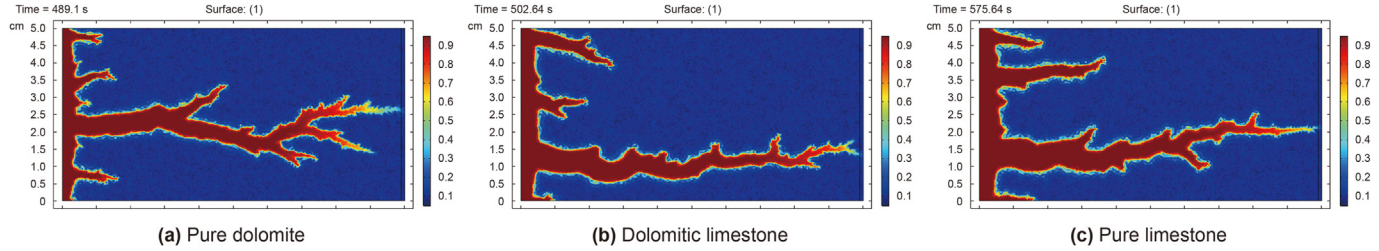

Fig. 15. Acid erosion porosity field for different orders of acid-rock reaction ($D_m = 9 \times 10^{-9}$ m^2·s^{-1}).

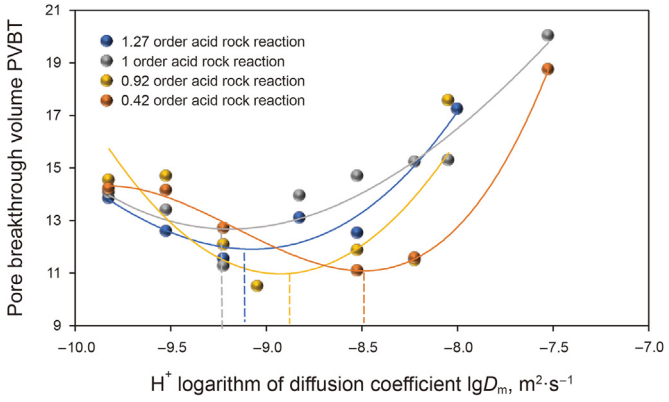

Fig. 16. Relative relationship between diffusion coefficient and breakthrough volume ratio for the multi-order acid-rock reaction H^+.

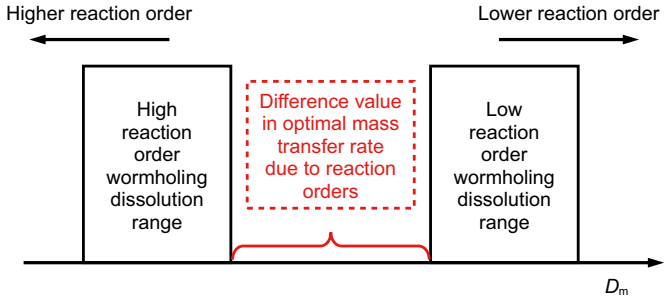

Fig. 17. Schematic diagram of multi-order acid-rock reaction dissolution patterns in relation to the range of injection rates.

the average value of actual acidification rate, mol·cm^{-2}·s^{-1}; $\hat{y}_i$ is the prediction of acidification rate value by numerical model, mol·cm^{-2}·s^{-1}.

After discretizing the curve data in Fig. 23, under the experimental conditions of this paper (4.4 mol·L^{-1} hydrochloric acid, 96% calcite content carbonate rock, 90 °C), the goodness of fit between the actual acid-rock reaction rate curve and the traditional model was calculated using the R^2 formula to be 63.58%, while the goodness of fit between the actual acid-rock reaction rate curve and the multi-order acid-rock reaction model was calculated to be 99.85%, resulting in an accuracy improvement of 36.27%.

Similarly, for carbonate rocks with 56% dolomite content, the fitting accuracy of the classic 1-order model is 93.07%, the fitting accuracy of the multi-order reaction model is 97.92%, and the accuracy is increased by 4.85%.

For the case where the dolomite content reaches 96%, the matching degree between the multi-order acid-rock reaction model and the actual reaction curve can reach 96.03%, but at this time, the R^2 score of the classic model and the actual reaction curve is negative, which indicates that the classic model has extremely poor accuracy when fitting the reaction order value deviates from the 1-order data to a large extent and further explains the adaptability of the multi-order reaction model to different reaction order models.

In general, the fitting accuracy of the multi-order acid-rock reaction model under different reaction orders is higher than that of the traditional model ($m \neq 1$). Under the carbonate acidizing conditions of three different mineral components simulated in this paper, the best fitting accuracy of the multi-order model can be as high as 99.85%, and the maximum accuracy increase can be as high as 36.27%, indicating that the multi-order reaction model can well reflect the real change of acidizing reaction rate under different reaction orders.

5. Conclusions

(1) Based on the traditional two-scale continuous medium model, this paper constructs a numerical model of acidification applicable to the calculation of multi-order acid-rock reactions using a function segmentation fitting method, which improves the accuracy of the calculation of the theoretical model of acidification when the number of acid-rock reaction orders is not one, the best fitting accuracy can reach 99.85%, and the maximum improvement of accuracy can reach 36.27%.

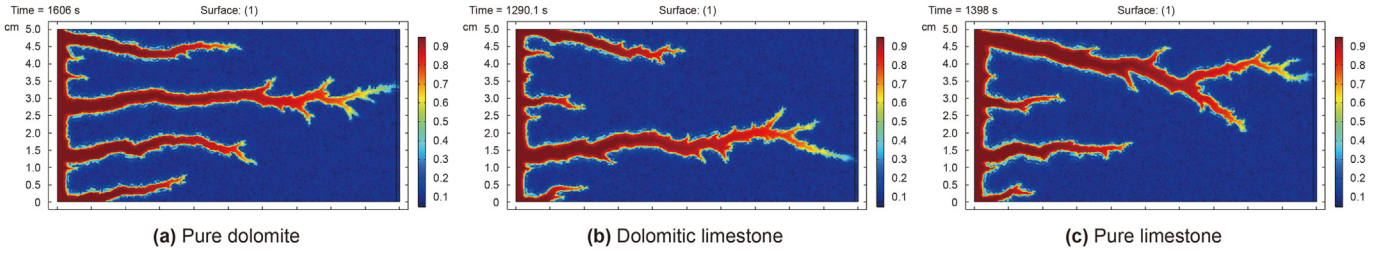

Fig. 18. Acid erosion porosity field for different orders of acid-rock reaction ($C_0 = 1.4$ mol·L^{-1}).

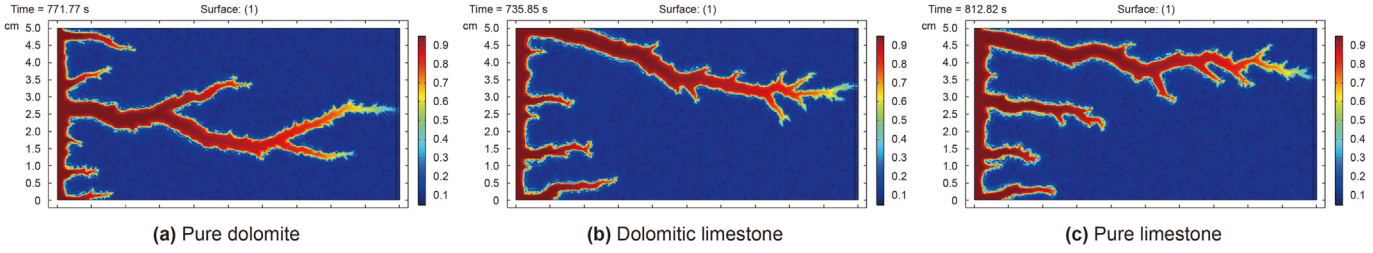

Fig. 19. Acid erosion porosity field for different orders of acid-rock reaction ($C_0 = 2.4$ mol·L^{-1}).

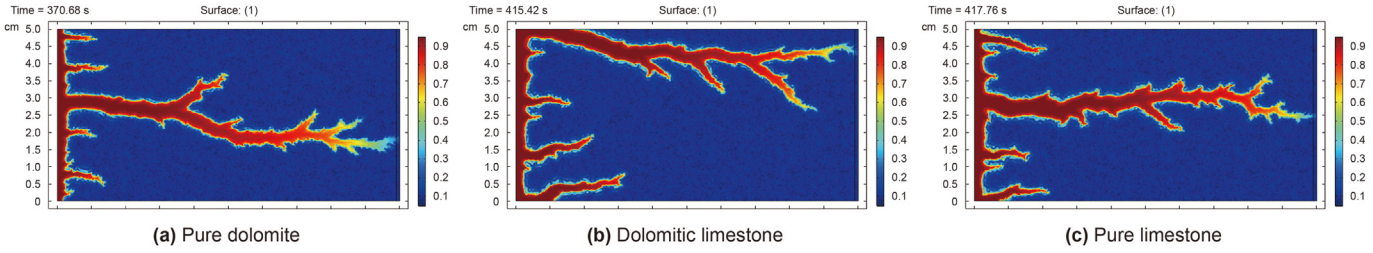

Fig. 20. Acid erosion porosity field for different orders of acid-rock reaction ($C_0 = 4.4$ mol·L^{-1}).

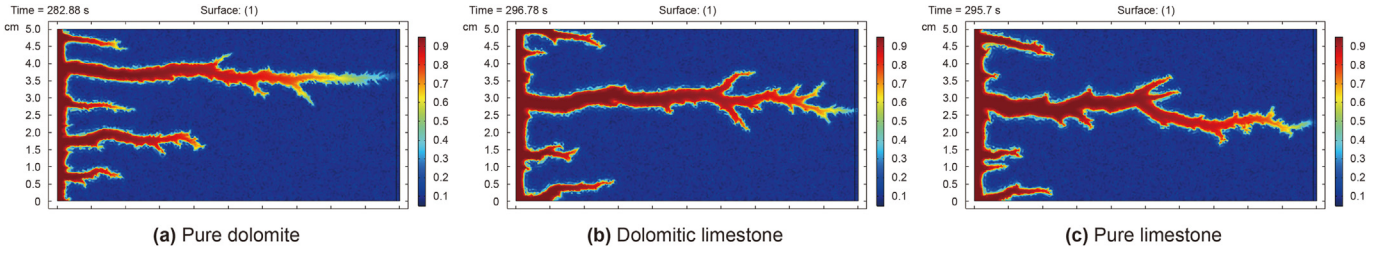

Fig. 21. Acid erosion porosity field for different orders of acid-rock reaction ($C_0 = 6.4$ mol·L^{-1}).

(2) The reaction order of carbonate rocks with 96% dolomite, 56% dolomite, and 96% calcite were 0.42, 0.92, and 1.27, respectively, and the reaction rates were 6.02×10^{-6} m·s^{-1}, 1.44×10^{-5} m·s^{-1} and 4.20×10^{-5} m·s^{-1}, respectively, under the experimental conditions of this paper. In the range of 5%–25% mass fraction of hydrochloric acid, the reaction rate of acid-rock accelerated and the non-uniform etching deepened as the number of reaction orders increased and the concentration of acid increased.

(3) Numerical simulations of multi-order acid-rock reactions show that the rock dissolution pattern changes from facet dissolution to wormholing dissolution to homogeneous dissolution as the acid flow rate increases. The H^+ diffusion coefficient increases and the rock dissolution pattern changes in the opposite direction. The higher the number of reaction orders, the higher the optimum acid flow rate and the lower the optimum H^+ diffusion coefficient required to form wormholes. However, the difference in breakthrough volume ratio curves with acid concentration is not significant for different reaction orders.

(4) The acidizing site should inject high viscosity acid in small volume and use slow acid systems such as thickening acid, cross-linking acid and emulsifying acid when reforming carbonate reservoir with high calcite content; and inject low viscosity acid in large volume and use conventional acid systems such as hydrochloric acid when reforming carbonate reservoir with high dolomite content. When the acid mass

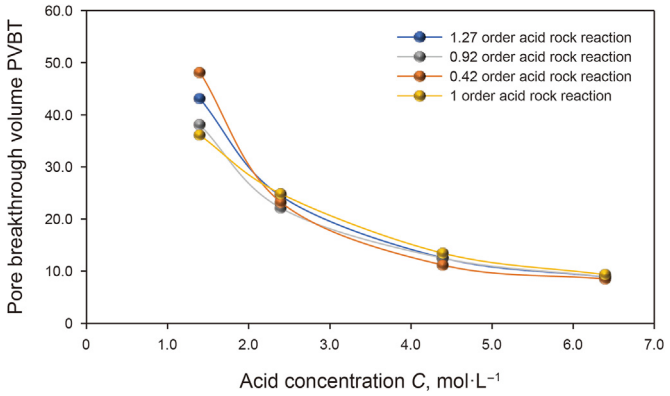

Fig. 22. Schematic diagram of acid concentration vs. acid volume ratio for multi-order acid-rock reaction.

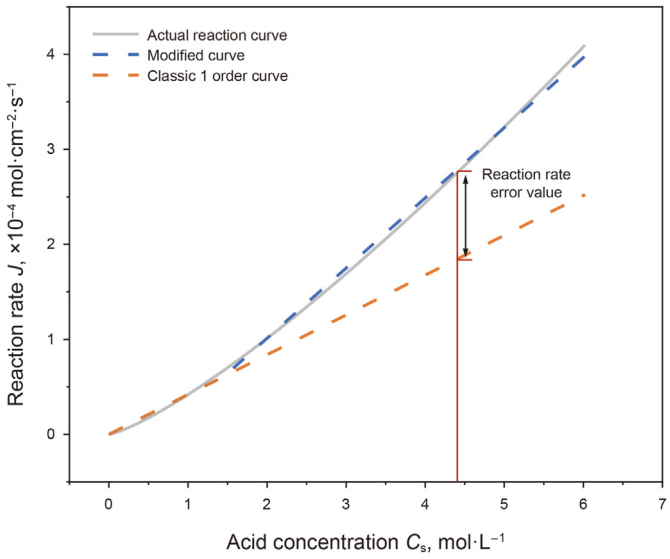

Fig. 23. Comparison of acid-rock reaction rate curves between the traditional primary model and the 1.27 order model.

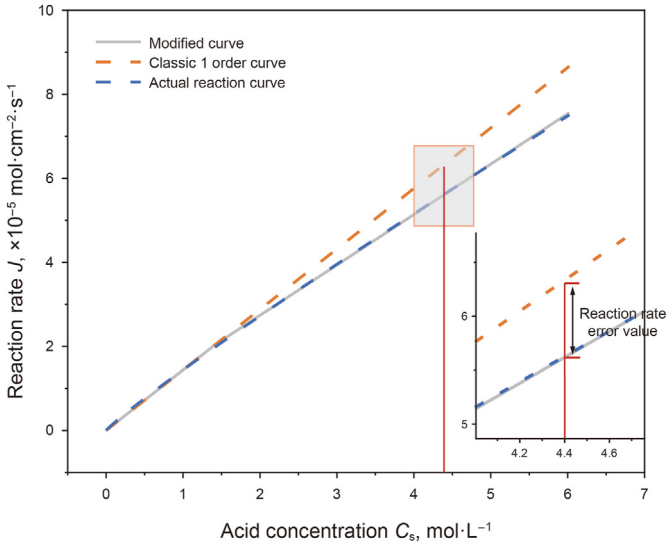

Fig. 24. Comparison of acid-rock reaction rate curves between the traditional primary model and the 0.92 order model.

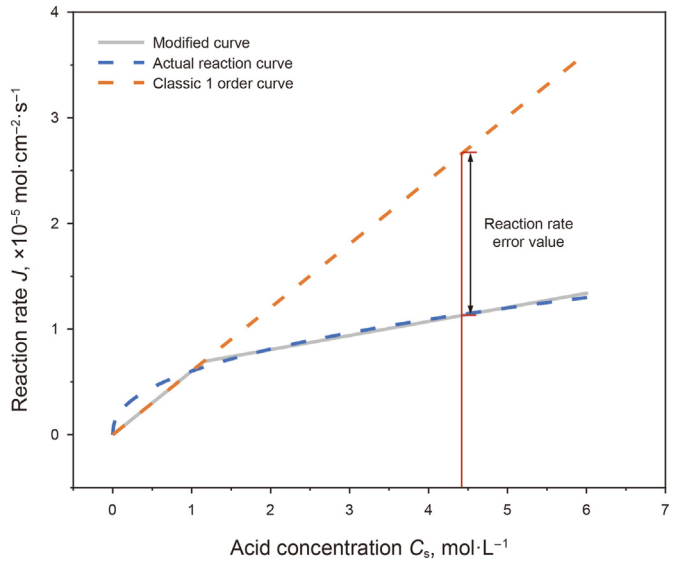

Fig. 25. Comparison of acid-rock reaction rate curves between the traditional primary model and the 0.42 order model.

fraction is less than 25%, an appropriate increase in acid concentration can improve the acidification efficiency.

Declaration of competing interest

The authors declare that they have no known competing financial interests or personal relationships that could have appeared to influence the work reported in this paper.

Acknowledgements

This work was financially supported by the National Natural Science Foundation of China (Project No. 51874336), the National Key Technologies Research and Development Program of China during the 13th Five-Year Plan Period (Project No. 2017ZX005030005). Their sponsorship is gratefully acknowledged.

References

Abdelgawad, K.Z., Mahmoud, M., Elkatatny, S., Abdulraheem, A., Patil, S., 2019. Reaction kinetics and coreflooding study of high-temperature carbonate reservoir stimulation using GLDA in seawater. Energies 12 (18), 3407. https://doi.org/10.3390/en12183407.

Al-Arji, H., Al-Azman, A., Le-Hussain, F., Regenauer-Lieb, K., 2021. Acid stimulation in carbonates: a laboratory test of a wormhole model based on Damköhler and Péclet numbers. J. Petrol. Sci. Eng. 203, 108593. https://doi.org/10.1016/j.petrol.2021.108593.

Algive, L., Bekri, S., Vizika, O., 2010. Pore-network modeling dedicated to the determination of the petrophysical-property changes in the presence of reactive fluid. SPE J. 15 (3), 618–633. https://doi.org/10.2118/124305-PA.

Baxter, E.F., Depaolo, D.J., 2002. Field measurement of high temperature bulk reaction rates II: interpretation of results from a field site near Simplon Pass, Switzerland. Am. J. Sci. 302 (6), 465–516. https://doi.org/10.2475/ajs.302.6.465.

Bickle, M.J., 1992. Transport mechanisms by fluid-flow in metamorphic rocks; oxygen and strontium decoupling in the Trois Seigneurs Massif; a consequence of kinetic dispersion? Am. J. Sci. 292 (5), 289–316. https://doi.org/10.2475/ajs.292.5.289.

Buijse, M.A., 2000. Understanding wormholing mechanisms can improve acid treatments in carbonate formations. SPE Prod. Facil. 15 (3), 168–175. https://doi.org/10.2118/65068-PA.

Chang, H.M., Xu, Y., Chen, S.S., He, Z., 2022. Enhanced understanding of osmotic membrane bioreactors through machine learning modeling of water flux and salinity. Sci. Total Environ. 838, 156009. https://doi.org/10.1016/j.scitotenv.2022.156009.

Chen, J., 2000. On the method of determining the number of reaction orders. University Chemistry 15 (6), 49–50. https://doi.org/10.3969/j.issn.1000-8438.2000.06.017 (in Chinese).

Chen, Y., Wang, H., Wang, Y., Ma, G., 2020. Numerical evaluation of a fracture acidizing treatment in a three-dimensional fractured carbonate reservoir. J. Nat. Gas Sci. Eng. 81, 103440. https://doi.org/10.1016/j.jngse.2020.103440.
Dong, K., 2018. A new wormhole propagation model at optimal conditions for carbonate acidizing. J. Petrol. Sci. Eng. 171, 1309–1317. https://doi.org/10.1016/j.petrol.2018.08.055.
Dong, R., Wheeler, M.F., Su, H., Ma, K., 2021. Modeling acid fracturing treatments in heterogeneous carbonate reservoirs. In: SPE International Conference on Oilfield Chemistry. The Woodlands, Texas, USA. December. https://doi.org/10.2118/204304-MS.
Dos Santos Lucas, C.R., Neyra, J.R., Araújo, E.A., da Silva, D.N.N., Lima, M.A., Ribeiro, D.A.M., Aum, P.T.P., 2022. Carbonate acidizing—A review on influencing parameters of wormholes formation. J. Petrol. Sci. Eng. 111168. https://doi.org/10.1016/j.petrol.2022.111168.
Fatt, I., 1956. The network model of porous media. Transactions of the AIME 207 (1), 144–181. https://doi.org/10.2118/574-G.
Fredd, C.N., Miller, M.J., 2000. Validation of carbonate matrix stimulation models. In: SPE International Symposium on Formation Damage Control. Lafayette, Louisiana, February. https://doi.org/10.2118/58713-MS
Guo, J., Zhan, L., Gou, B., Zeng, J., Zhou, C., 2020. Experimental optimization of acid system for acidizing in mud-damaged deep fractured carbonate formation. J. Petrol. Sci. Eng. 195, 107639. https://doi.org/10.1016/j.petrol.2020.107639.
Hoefner, M.L., Fogler, H.S., 1989. Fluid-velocity and reaction-rate effects during carbonate acidizing: application of network model. SPE Prod. Eng. 4 (1), 56–62. https://doi.org/10.2118/15573-PA.
Hoff, J.H., 1884. Etudes de dynamique chimique. Recl. Trav. Chim. Pays-Bas 3 (10), 333–336. https://doi.org/10.1002/recl.18840031003.
Hung, K.M., Hill, A.D., Sepehrnoori, K., 1989. A mechanistic model of wormhole growth in carbonate matrix acidizing and acid fracturing. J. Petrol. Technol. 41 (1), 59–66. https://doi.org/10.2118/16886-PA.
Jia, C., Sepehrnoori, K., Huang, Z., Zhang, H., Yao, J., 2021. Numerical studies and analysis on reactive flow in carbonate matrix acidizing. J. Petrol. Sci. Eng. 201, 108487. https://doi.org/10.1016/j.petrol.2021.108487.
Kamble, R.G., Raykar, N.R., Jadhav, D.N., 2021. Machine learning approach to predict fatigue crack growth. Mater. Today: Proc. 38, 2506–2511. https://doi.org/10.1016/j.matpr.2020.07.535.
Lasaga, A.C., 1986. Metamorphic reaction rate laws and development of isograds. Mineral. Mag. 50 (357), 359–373. https://doi.org/10.1180/minmag.1986.050.357.02.
Liu, X., Ormond, A., Bartko, K., Ying, L., Ortoleva, P., 1997. A geochemical reaction-transport simulator for matrix acidizing analysis and design. J. Petrol. Sci. Eng. 17 (1–2), 181–196. https://doi.org/10.1016/S0920-4105(96)00064-2.
Liu, P., Yan, X., Yao, J., Sun, S., 2019. Modeling and analysis of the acidizing process in carbonate rocks using a two-phase thermal-hydrologic-chemical coupled model. Chem. Eng. Sci. 207, 215–234. https://doi.org/10.1016/j.ces.2019.06.017.
Lohrasb, S., Junin, R., Agi, A., 2022. Evaluation of an empirical model for pore volume to breakthrough and wormhole growth in carbonate acidizing. Petrol. Sci. Technol. 1–19. https://doi.org/10.1080/10916466.2022.2156540.
Ma, J., Xie, S., Tang, H., Ma, M., Carranza, E.J.M., Han, J., Zhang, H., 2020. Evolution mechanisms of carbonate reservoirs based on dissolution rates and multifractal analysis of microscopic morphology. Nat. Resour. Res. 29, 2843–2865. https://doi.org/10.1007/s11053-020-09645-z.
Ma, G., Chen, Y., Wang, H., Li, T., Nie, W., 2022. Numerical analysis of two-phase acidizing in fractured carbonate rocks. J. Nat. Gas Sci. Eng. 103, 104616. https://doi.org/10.1016/j.jngse.2022.104616.
Maheshwari, P., Ratnakar, R.R., Kalia, N., Balakotaiah, V., 2013. 3-D simulation and analysis of reactive dissolution and wormhole formation in carbonate rocks. Chem. Eng. Sci. 90, 258–274. https://doi.org/10.1016/j.ces.2012.12.032.
Mahmoodi, A., Javadi, A., Sola, B.S., 2018. Porous media acidizing simulation: new two-phase two-scale continuum modeling approach. J. Petrol. Sci. Eng. 166, 679–692. https://doi.org/10.1016/j.petrol.2018.03.072.
Martyushev, D.A., Vinogradov, J., 2021. Development and application of a double action acidic emulsion for improved oil well performance: laboratory tests and field trials. Colloids Surf. A Physicochem. Eng. Asp. 612, 125998. https://doi.org/10.1016/j.colsurfa.2020.125998.
Martyushev, D.A., Govindarajan, S.K., Li, Y., Yang, Y., 2022. Experimental study of the influence of the content of calcite and dolomite in the rock on the efficiency of acid treatment. J. Petrol. Sci. Eng. 208, 109770. https://doi.org/10.1016/j.petrol.2021.109770.
Morse, J.W., Arvidson, R.S., Lüttge, A., 2007. Calcium carbonate formation and dissolution. Chem. Rev. 107 (2), 342–381. https://doi.org/10.1021/cr050358j.
Panga, M.K., Ziauddin, M., Balakotaiah, V., 2005. Two-scale continuum model for simulation of wormholes in carbonate acidization. AIChE J. 51 (12), 3231–3248. https://doi.org/10.1002/aic.10574.
Papamichos, E., Strongylis, P., Bauer, A., 2020. Reactive instabilities in linear acidizing on carbonates. Geomechanics for Energy and the Environment 21, 100161. https://doi.org/10.1016/j.gete.2019.100161.
Qi, N., Li, B., Chen, G., Fang, M., Li, X., Liang, C., 2017. Optimum fluid injection rate in carbonate acidizing based on acid dissolution morphology analysis. Energy & Fuels 31 (12), 13448–13453. https://doi.org/10.1021/acs.energyfuels.7b02674.
Qi, N., Chen, G., Fang, M., Li, B., Liang, C., Ren, X., Zhang, K., 2018. Damköhler number-based research on dividing dissolution patterns in carbonate acidizing. J. Petrol. Sci. Eng. 170, 922–931. https://doi.org/10.1016/j.petrol.2018.06.070.
Qiu, X., Edelman, E., Aidagulov, G., Ghommem, M., Brady, D., Abbad, M., 2018. Experimental investigation of radial and linear acid injection into carbonates for well stimulation Operations. In: SPE Kingdom of Saudi Arabia Annual Technical Symposium and Exhibition. OnePetro. https://doi.org/10.2118/192261-MS.
Sahu, Q., Fahs, M., Hoteit, H., 2022. Optimization and uncertainty quantification method for reservoir stimulation through carbonate acidizing. ACS Omega 8 (1), 539–554. https://doi.org/10.1021/acsomega.2c05564.
Skelton, A., 2011. Flux rates for water and carbon during greenschist facies metamorphism. Geology 39 (1), 43–46. https://doi.org/10.1130/G31328.1.
Skelton, A.D.L., Bickle, M.J., Graham, C.M., 1997. Fluid-flux and reaction rate from advective-diffusive carbonation of mafic sill margins in the Dalradian, southwest. Earth and Planetary Science Letters 146 (3-4), 527–539. https://doi.org/10.1016/S0012-821X(96)00248-8.
Su, X., Qi, N., Shi, X., Yang, X., Deng, D., Li, X., 2022. Two-scale continuum model for simulation of acid fracturing in carbonate reservoirs with two main mineral components. AIChE J. 68 (8), e17712. https://doi.org/10.1002/aic.17712.
Tabasy, M., Rashidi, F., 2015. A qualitative simulation of a face dissolution pattern in acidizing process using rotating disk apparatus for a carbonate gas reservoir. J. Nat. Gas Sci. Eng. 26, 1460–1469. https://doi.org/10.1016/j.jngse.2015.08.014.
Tansey, J., Balhoff, M.T., 2016. Pore network modeling of reactive transport and dissolution in porous media. Transport Porous Media 113, 303–327. https://doi.org/10.1007/s11242-016-0695-x.
Waldmann, P., 2019. On the use of the Pearson correlation coefficient for model evaluation in genome-wide prediction. Front. Genet. 10, 899. https://doi.org/10.3389/fgene.2019.00899.
Wang, L., Mou, J., Mo, S., Zhao, B., Liu, Z., Tian, X., 2020. Modeling matrix acidizing in naturally fractured carbonate reservoirs. J. Petrol. Sci. Eng. 186, 106685. https://doi.org/10.1016/j.petrol.2019.106685.
Wei, W., Varavei, A., Sanaei, A., Sepehrnoori, K., 2019. Geochemical modeling of wormhole propagation in carbonate acidizing considering mineralogy heterogeneity. SPE J. 24 (5), 2163–2181. https://doi.org/10.2118/195593-PA.
Wilhelmy, L., 1850. The law by which the action of acids on cane sugar occurs. Annalen Physik Chemie 81, 413–433.
Xue, H., 2017. Research on Numerical Simulation of Efficient Acidification of Horizontal Wells in Complex Carbonate Rock Reservoirs. Doctoral Dissertation. Southwest Petroleum University. CNKI: CDMD: 1.1018.021277 (in Chinese).
Yan, Y.L., Xi, Q., Una, C.C., He, B.C., Wu, C.S., Dou, L.L., 2019. A novel acidizing technology in carbonate reservoir: in-Situ formation of CO_2 foamed acid and its self-diversion. Colloids Surf. A Physicochem. Eng. Asp. 580, 123787. https://doi.org/10.1016/j.colsurfa.2019.123787.
Yoo, H., Kim, Y., Lee, W., Lee, J., 2018. An experimental study on acid-rock reaction kinetics using dolomite in carbonate acidizing. J. Petrol. Sci. Eng. 168, 478–494. https://doi.org/10.1016/j.petrol.2018.05.041.
Zhou, L., Guo, A., Wang, X., Qiao, J., Tang, X., 2022. The effect of temperature, natural fractures and vugs on the acidizing process in fractured-vuggy reservoirs with hydro-thermal-chemical coupled modeling. J. Petrol. Sci. Eng. 213, 110416. https://doi.org/10.1016/j.petrol.2022.110416.